Investigation of time-dependent forces on a nano-Newton-second impulse balance

Brian C. D'Souza
University of Southern California, Department of Aerospace and Mechanical Engineering, Los Angeles, California 90089-1191

Andrew D. Ketsdever
Air Force Research Laboratory, Propulsion Directorate, Edwards Air Force Base, California 93524

(Received

A torsional impulse balance has been developed as a new diagnostic tool to study fundamental physical processes in micropropulsion systems and laser-surface interactions. The impulse balance has been designed and tested with a robust calibration system to measure impulsive forces with resolution as low as several nano-Newton-seconds. The behavior of the impulse balance was thoroughly studied and characterized. A simple analytical model of the balance's motion was developed from the general equation of motion of an underdamped, harmonically oscillating system. Also, two distinct methods of analyzing the experimental data from the nano-impulse balance have been investigated. The first method resolves the total impulse as a function of the balance's maximum deflection. The second method enables the determination of the impulse and/or force applied as a function of time from the balance's time-resolved motion. A calibration scheme employing electrostatic actuation techniques is used to experimentally validate the model and impulse measurement techniques.

Report Documentation Page

Form Approved
OMB No. 0704-0188

1. REPORT DATE	2. REPORT TYPE	3. DATES COVERED
25 MAR 2004		**-**

4. TITLE AND SUBTITLE	5a. CONTRACT NUMBER
Investigation of Time-Dependent Forces on a Nano-Newton-Second Impulse Balance	5b. GRANT NUMBER
	5c. PROGRAM ELEMENT NUMBER
6. AUTHOR(S)	5d. PROJECT NUMBER
	5e. TASK NUMBER
	5f. WORK UNIT NUMBER
7. PERFORMING ORGANIZATION NAME(S) AND ADDRESS(ES) **Air Force Research Laboratory (AFMC),AFRL/PRS,5 Pollux Drive,Edwards AFB,CA,93524-7048**	8. PERFORMING ORGANIZATION REPORT NUMBER
9. SPONSORING/MONITORING AGENCY NAME(S) AND ADDRESS(ES)	10. SPONSOR/MONITOR'S ACRONYM(S)
	11. SPONSOR/MONITOR'S REPORT NUMBER(S)

12. DISTRIBUTION/AVAILABILITY STATEMENT
Approved for public release; distribution unlimited

13. SUPPLEMENTARY NOTES

14. ABSTRACT

A torsional impulse balance has been developed as a new diagnostic tool to study fundamental physical processes in micropropulsion systems and laser-surface interactions. The impulse balance has been designed and tested with a robust calibration system to measure impulsive forces with resolution as low as several nano-Newton-seconds. The behavior of the impulse balance was thoroughly studied and characterized. A simple analytical model of the balanceŸs motion was developed from the general equation of motion of an underdamped, harmonically oscillating system. Also, two distinct methods of analyzing the experimental data from the nanoimpulse balance have been investigated. The first method resolves the total impulse as a function of the balanceŸs maximum deflection. The second method enables the determination of the impulse and/or force applied as a function of time from the balanceŸs time-resolved motion. A calibration scheme employing electrostatic actuation techniques is used to experimentally validate the model and impulse measurement techniques.

15. SUBJECT TERMS

16. SECURITY CLASSIFICATION OF:			17. LIMITATION OF ABSTRACT	18. NUMBER OF PAGES	19a. NAME OF RESPONSIBLE PERSON
a. REPORT	b. ABSTRACT	c. THIS PAGE			
unclassified	**unclassified**	**unclassified**		**40**	

I. INTRODUCTION

Several impulse balances have been designed to measure transient forces produced by a variety of processes.[1-3] Generally, the impulse generated by a device is investigated by measuring the maximum deflection of the balance caused by a given impulse.[2,3] There are two major shortcomings of this approach. First, there is no information that can be inferred from this data regarding the pulse width, τ, or the pulse shape. Second, it is only strictly valid for $\tau \ll T$. Since very different pulse widths and shapes can lead to the same maximum deflection on an impulse balance, the simple method of investigating a balance's maximum deflection is not adequate to determining the characteristics of the impulse delivered. A detailed analysis of the impulse balance's equation of motion can lead to a more complete understanding of the complex physical processes which may be driving device operation.

There are a number of applications of current interest where the knowledge of time resolved forces would be beneficial to the basic understanding of physical processes. Two of these applications are spacecraft propulsion and laser ablation. For spacecraft propulsion, fine attitude control requires precise and reproducible impulse delivery from the thruster system. Although total delivered impulse is generally measured and deemed adequate for most mission scenarios, time resolved thrust measurements would be beneficial in understanding the physics of thruster operation and could lead to the development of more precise and efficient thruster systems. For example, pulsed plasma thrusters (PPT) use a spark generated across a Teflon propellant to produce an energetic arc-ablated ionized plume.[4] The total impulse delivery from a PPT involves a relatively low mass of highly energetic ions and a large mass of slow moving

molecules and heavier particles as shown schematically in Fig. 1a. The initially ablated material produces the majority of the thrust. Subsequent heat adsorption by the Teflon produces a late-time ablative plume of relatively massive, slow moving molecules and particles.[5] The late-time ablation does not produce significant thrust; however, a relatively large amount of propellant mass is lost in this process leading to thruster inefficiencies. Although the total impulse, $\mathcal{I}$, obtained from integrating F(t) versus time in Fig. 1a and Fig. 1b are the same, the detailed physics behind the production of each impulse curve may be quite different. A simple analysis based on the balance maximum deflection would not yield any information about the pulse shape. The investigation of the time dependent forces produced by a PPT can lead to more efficient thrusters by investigating system changes that maximize the efficient production of ionized propellant and minimize the production of late-time ablation. A measure of propulsive efficiency is the specific impulse, I_{sp}, given by

$$I_{sp} = \frac{1}{M_p g_o} \int_{t=0}^{t=t'} F(t)dt \qquad (1)$$

where F(t) is the time dependent force produced by the thruster, t' is the thruster's pulse duration, and M_p is the total mass of the propellant lost in the pulse, and g_o is the Earth's gravitational constant. From Eq. (1), it can be seen that details of the impulse delivery in the integral are important for thruster efficiency.

Within the scope of laser ablation, investigations of a wide variety of physical processes, which include sputtering, vaporization, ionization, and gas desorption, are of interest.[6] The conditions under which each physical process might occur and the parameters which may control each process can be studied by time resolved force measurements. For example, an investigation of the onset of sputtering as a function of laser energy or pulse duration can be performed. At

relatively low laser energy and long pulsewidth, gas desorption, due to the rapid heating of the surface, is expected to be the dominant impulse producing process. As the laser energy increases and/or the pulse duration decreases, material sputtering or ionization may become dominant.[7] Through a careful investigation of the time resolved forces produced in the photon-surface interactions, the energy corresponding to the onset of sputtering for a particular material may be identified.

The scope of this work was three fold. First, a uniquely successful nano-Newton-second impulse balance system (NIBS) capable of resolving total impulse measurements as low as 7 nano-Newton-seconds (nNs) was designed and constructed. Second, an analytical model was developed from the equations of motion for an underdamped, harmonically oscillating system. The model was validated using experimental data obtained from the NIBS. Finally, a data reduction method to accurately time-resolve the applied force from the NIBS deflection data was developed. The developed model and data reduction methods in this study are extended to impulse balance operation for arbitrary pulsewidth (i.e. with no restriction on the pulsewidth duration relative to the natural motion of the stand).

II. NANO-IMPULSE BALANCE SYSTEM

The current version of the NIBS is based upon a torsional thrust stand developed jointly by the Air Force Research Laboratory and the University of Southern California.[8] The NIBS design has been modified to allow for very low impulse measurements, which could not be attained by previous versions of the stand. An electrostatic comb force calibration technique described by

Selden and Ketsdever[9] has been employed to accurately calibrate the system for transient impulses.

As shown in Fig. 2, the NIBS is a torsional pendulum with viscous damping. Two flexure pivots provide the restoring force for the system with a combined rotational spring constant of approximately 0.200Nm/rad (measured). The entire structure is made of aluminum to keep the balance's moment of inertia as low as possible in an attempt to maximize the deflection for a given applied force. The arms were fabricated from square tubing to provide rigidity over long lengths, and channels were cut from the side of the tubing to reduce mass. Propulsion systems or test materials are mounted at the end of the 46 cm long arms. The Electrostatics Force Calibration System (EFCS) is mounted on the end of one arm at the same location from the center of rotation as the impulse delivery is expected. The NIBS motion is sensed by a linear variable differential transducer (LVDT). The LVDT senses a linear motion at the end of the balance's arm, which can be transformed into a rotational deflection. The data trace obtained by monitoring the LVDT output over time provides the basis for deriving the impulse imparted to the NIBS. A damping cup is mounted to the bottom of the NIBS and is placed in an oil bath to provide viscous damping, which is essential for damping out the motion of the stand in vacuum.

III. IMPULSE BALANCE MODEL

The motion of an underdamped, harmonically oscillating system can be expressed in rotational or linear terms by the following

$$I\ddot{\theta}(t) + C\dot{\theta}(t) + K\theta(t) = F(t)r = M(t) \tag{2}$$

$$I\ddot{x}(t) + C\dot{x}(t) + Kx(t) = F(t)r^2 = M(t)r$$

The angular solutions can easily be transformed into a linear deflection to correspond to the measurement methods used in the experimental setup. For the general case of forced motion of an underdamped system, consider M(t) = M_o to be constant over a defined time period (pulse width) τ, as shown in Fig. 1b. This can be representative of either a constant impulse or steady-state situation, depending on the length of τ. The solution to Eq. (2) for initial conditions of angular displacement θ_o and angular velocity $\dot{\theta}_o$ is[10]

$$\theta(t) = \frac{M_o}{K} + e^{\alpha t}\left[\left\{\theta_o - \frac{M_o}{K}\right\}\cos\beta t + \left\{\frac{\dot{\theta}_o K - \alpha K\theta_o + \alpha M_o}{K\beta}\right\}\sin\beta t\right] \tag{3}$$

$$\dot{\theta}(t) = e^{\alpha t}\left[\dot{\theta}_o\cos\beta t + \left\{\frac{I\alpha\dot{\theta}_o - K\theta_o + M_o}{I\beta}\right\}\sin\beta t\right] \tag{4}$$

$$\ddot{\theta}(t) = e^{\alpha t}\left[\left\{\frac{M_o - C\dot{\theta}_o - K\theta_o}{I}\right\}\cos\beta t + \left\{\frac{\alpha\left(M_o - C\dot{\theta}_o - K\theta_o\right) - K\dot{\theta}_o}{I\beta}\right\}\sin\beta t\right] \tag{5}$$

where $\alpha = -C/2I = -\delta/T$ and $\beta = [K/I - \alpha^2]^{1/2}$. Note that by removing the damping term, the expected natural frequency $\omega_n = [K/I]^{1/2}$ for a simple torsional spring is obtained.

A closed-form analytical solution of the equation of motion in Eq. (2) is not possible for any arbitrary applied moment, M(t). However, the problem may be broken up into segments. Any arbitrary or irregular force can be reasonably approximated using a series of constant force segments of small time widths $d\tau$. The initial conditions of any given segment are simply the end state of the displacement and velocity terms from the previous segment.

Equations (3-5) have been used to develop a simple software tool that has been validated using experimental data. The software has been used to examine the expected behavior of the NIBS for impulses of varying pulse widths and for steady state operations. Figure 3 shows a comparison of NIBS experimental data for a 242 nNs impulse with the analytical model. Figure 3 shows good agreement between the model and experimental data for the magnitude and frequency of the balance's motion.

IV. SIGNAL PROCESSING AND DATA REDUCTION

A. Wavelet And Fourier Transform Denoising

The ability to obtain reliable and repeatable force measurements from NIBS depends on the time-varying deflection traces provided by the LVDT. The LVDT sensor provides an analog output, which commonly exhibits significant high frequency noise components. The noise can mostly be attributed to electrical sources (primarily in the 15Hz, 50Hz and 60Hz ranges). Two signal analysis techniques have been employed in this study to perform denoising of the LVDT signal: Fourier and wavelet transforms.

First, the Fourier transform $F(\omega)$ of a given signal $f(t)$ deconstructs the signal into constituent sinusoidal components. Fourier signal analysis techniques are fairly common and numerous tools exist to facilitate the transform of a given signal into a frequency spectrum. The denoising technique employed was a simple frequency thresholding, whereby all components higher than a specified frequency are filtered out. This technique essentially functions as an ideal low-pass

filter (LPF).[11] The signal can then be transformed back from the frequency domain into the time domain for further data reduction and analysis.

While the principal frequency of interest is the effective frequency of the NIBS, care must be taken in choosing a threshold frequency. Selecting too low of a threshold frequency may result in the loss of actual signal, which would typically result in the undervaluing of the derived impulse. For sets of data that were analyzed using the Fourier techniques, the threshold frequency used was 10 Hz.

Alternately, the wavelet transform has also proved to be a valuable tool for denoising and smoothing of the raw experiment data. The wavelet transform is analogous to Fourier transforms in that it decomposes a signal into coefficients of constituent waveforms. However, Fourier analysis depends entirely on decomposition by sinusoids across the frequency spectrum. Wavelet analysis allows for the waveform to be of any arbitrary shape and decomposes the signal across the time domain. The coefficients of the wavelet transform are a function of scale and position (shift in time).[12]

The decomposition by scale and position allows for the isolation of successive levels of small scale structure or detail, leaving the remaining portion as an approximation of the original signal. Applying thresholding settings to these detail coefficients can result in removing general noise components while leaving actual fine structure intact. Such a deconstruction into scale and time domains can provide valuable information about the signal through inspection of the coefficients, as anomalous points and localized events are often clearly evident. Also, since the transform

remains in the time domain, it is also possible to perform wavelet analysis on finite or shifting segments of a data set. This can be an extremely useful in handling large data sets. The major drawback of the wavelet process is that it can be extremely computationally intensive.

Both transform methods have been demonstrated to be quite reliable for deriving the total impulse from the deflection data. In either case, attention must be paid to not filter out more than just the noise from the signals. Figure 4 shows a comparison between the Fourier and wavelet denoising techniques for a typical deflection trace. Agreement between the Fourier and wavelet processed signals is excellent. Furthermore, the comparison of the derived impulse from such traces processed with Fourier and wavelet techniques resulted in differences less than 1%.

B. Time-Resolved Impulse Measurement Process

Once the raw data has been denoised through either the Fourier and/or wavelet transform methods, it can be used to derive the total impulse that was imparted to the NIBS. In the simplest case, for $\tau \ll T$, the total impulse may be derived from the maximum deflection. Calibration curves for this method can readily be derived, as will be shown in Section VI. However, the real interesting details of the impulse or force applied are the time resolved characteristics. The Time-Resolved Impulse Measurement (TRIM) process is derived from Eq. (2). The equation of motion for the NIBS indicates that the force applied (as a function of time) is simply related to the addition of the position, velocity and acceleration components, which are scaled by the spring constant K, damping coefficient C, and the moment of inertia I, respectively as shown in Fig. 5.

Since the position (deflection) as a function of time is measured in the experiments, the derivative of the data must simply be taken once to obtain the velocity and twice for the acceleration. The major problem here is resolving the derivatives for a signal with noise. Using the signal processing methods previously described, the raw position data can be cleaned up significantly. In addition, a Savitzky-Golay algorithm is used to take the derivatives. This algorithm employs a moving window over which the points are fitted for a line. The slope of the line represents the derivative of the point at the center of the window. This method results in artifacts at the beginning and end of a data trace. This method also tends to introduce slight aliasing effects, depending on the size of the window. However, it reliably maintains the content under the curve, which is essential for calculating the total impulse.

To complete the process, we need to determine I, C and K. The moment of inertia of the NIBS can be determined through a combination of physical measurement and CAD analysis. The spring constant and damping coefficient can then be determined from the position data by extracting the period of the oscillations T and the damping ratio δ, which is obtained from the natural logarithm of the ratio of successive peaks in the displacement data, $\delta = \ln[x_{max1}/x_{max2}]$. For completeness, it is also necessary to remember to include the term for the moment arm in Eq. (2). Finally, from the derived force F(t), the total impulse $\mathcal{I}(t)$ is given by integrating F(t).

V. EXPERIMENTAL SETUP AND PROCEDURE

The NIBS was installed in a 41 cm diameter x 122 cm long, stainless steel vacuum chamber fitted with a 450 L/sec turbomolecular pump capable of maintaining pressures of approximately

2 x 10^{-6} Torr. For this study, impulse delivery to the NIBS is accomplished by supplying a potential difference to the EFCS. The EFCS consisted of either an aluminum parallel plate assembly[2] or an aluminum comb assembly[9] with one side of the EFCS assembly attached directly to the NIBS. As shown in the experimental setup in Fig. 6, the power supply for the EFCS was attached to a pulse generator capable of delivering ±3500 V with a 20 ns rise time and a variable DC pulse width (minimum of 60 ns). The output of the pulse generator was sent directly to the EFCS assembly in the chamber through a high voltage vacuum feedthrough and was monitored by a 16-bit data acquisition (DAQ) system with a maximum sample rate of 333kHz. The applied (and monitored) voltage to the EFCS was used to calculate the actual time-dependent force applied to the NIBS.[9]

The actual forces applied were later compared to the force derived from the NIBS deflection data through the TRIM process described in Section IV-B. The motion of the NIBS was measured using an LVDT, which was connected to either a 16 or 24-bit data acquisition system. The 24-bit system used was limited to a sampling rate of 60 Hz, and the 16-bit system was capable of sampling at 333 kHz. In some of the tests, a simple low-pass filter (LPF) was used on the LVDT signal to minimize electrical noise. The analog filtering serves to complement the signal processing techniques discussed in Section IV-A. The raw data was filtered to reduce the noise in the experimental data, and the denoised data was differentiated to provide NIBS velocity and acceleration information, which was used to determine the characteristics of the delivered impulse as described in the previous section. Values of T and δ were obtained using NIBS displacement data. From these parameters and the measured moment of inertia, the values of the

damping (C) and spring (K) coefficients were calculated. Table 1 shows the characteristic values for the NIBS in this study.

VI. RESULTS

A. Calibration

Calibration of the NIBS was a critical element of this study. The application of a variety of known impulses of different magnitudes and pulsewidths were tested to demonstrate the stability and repeatability of the NIBS. From these tests, a process has been developed which allows the balance to be well characterized under any configuration.

In order to use the LVDT voltage output to obtain a derived impulse, a calibration factor is required that converts the analog voltage signals into appropriate displacement measurements. The LVDT was independently calibrated from repeated measurements in a staged micrometer configuration that spanned the full range of the LVDT. The conversion factor was determined to be 1453.366 V/m for the tested configuration, which included the use of a LPF for analog signal conditioning. For test configurations without the use of a LPF, an additional scaling factor of 1.0902 was necessary to compensate for the signal attenuation caused by the LPF.

The applied impulse is the known impulse delivered to the stand using the EFCS. The voltage applied to the EFCS is typically greater than 100V and is monitored and known to within 0.1V. The actual force produced by the EFCS was independently calibrated by the microbalance method described by Selden and Ketsdever.[9] The error for a given applied force was found to

be less than 2%. For all results presented in this paper, this error is understood to be present in all applied forces and impulses, whether or not it is visible in the figures or explicitly stated in the values.

Figure 7 shows three sets of dissimilar calibration data that was analyzed using appropriate calibration factors. One set of data was originally sampled at 9000Hz, the next was 1000Hz data, and the third was 1000Hz with the use of an analog LPF. Each of the sets show reasonable agreement with expected results as the derived impulses are consistently within 4.5% of the applied impulse. Each calibration data set also shows trends of being consistently slightly high or low, which would be consistent with filtering variations for each of the sets of data. This suggests that for any configuration of the NIBS, a consistent set of calibration data could be used with a consistent signal processing parameter to obtain appropriate calibration factors for an unknown impulse, which could minimize error in the derived impulse. Nevertheless, without any additional correction factors, the results for derived impulse throughout the paper repeatedly fall within 4.5% of the applied impulse.

B. Maximum Deflection Analysis

Figure 8 shows the NIBS maximum linear deflection as a function of applied impulse. The analytical model is in good agreement with the experimental data as shown in Fig. 8. For the cases presented in Fig. 8, the impulse pulsewidths (τ) were shorter than approximately one-tenth of the period (T) of the NIBS. Typically, impulse balances are operated using the assumption that the maximum deflection is linearly dependent on the delivered impulse.[2,3] The assumption is only strictly valid for $\tau \ll T$. Figure 9 shows the maximum NIBS deflection as a function of τ /

T for various total impulses. The analytical model captures not only the trend of the experimental data, but is also in excellent agreement with the magnitude of the data. As seen in Fig. 9 for $\tau > 0.1$ T, the direct correlation between the maximum balance displacement and the delivered impulse is no longer valid. For $\tau \ll$ T, the maximum deflection has a linear relationship with the total impulse as shown in Fig. 8. For larger τ, there are two possible scenarios. First, two different total impulses (say one with $\tau \ll$ T and one with $\tau \sim$ T) can lead to the same maximum deflection; second, two identical total impulses with different pulsewidth can result in different maximum deflection. Examples of these two scenarios will be shown in Section VI-C. Therefore, another means by which to analyze the data is necessary if the pulsewidth is not known a priori.

C. Derived Impulse Analysis

Figure 10a shows the impulse balance deflection as a function of time for two impulses of the same total magnitude (integrated force with time). The maximum deflection from the NIBS is not the same even though the total impulse is identical for both cases. The actual time varying force applied is shown by the dashed line in Fig. 10b. As shown, the pulsewidth of the two traces was different by an order of magnitude. The TRIM process described in Section IV-B was used to obtain the derived time varying force also shown in Fig. 10b. Figure 10c shows the total impulse delivered to the balance obtained by the integral under the curves in Fig. 10b. Although the maximum deflection for the two pulses was not the same, Fig. 10c shows that the total impulse delivered were in fact identical.

Figure 11a shows the NIBS linear displacement versus time for impulses of 42.34 μNs and 21.65 μNs. The pulsewidths for these impulses was 1.55 sec and 0.1 sec respectively. As seen in Fig. 10a, the maximum NIBS deflection is the same for both impulses even though the total impulses are different by a factor of two. Figure 10b shows the impulse shape for both cases. The dashed lines are from the signal delivered by the pulse generator, and the solid lines are derived from the filtered NIBS deflection data using the TRIM data reduction technique described in Section IV-B. As Fig. 11b indicates, there are system time response issues that would not allow better resolution of the impulse shape with faster data acquisition sampling. The time response of the LVDT signal-conditioning unit was seen to be less than 100 Hz, which was generally not fast enough to adequately resolve the impulse shape for very short pulsewidths due to aliasing. However, the total impulse taken as the integral under both curves (pulse generator, LVDT derived) is the same to within 4.5% as shown in Fig. 11c. Although the maximum displacement of the NIBS was the same for the two impulses (as shown in Fig. 11a), the total impulse was indeed a factor of two different as shown in Fig. 11c.

Figure 12a shows the experimentally derived force from the NIBS as a function of time for an impulse comprised of two square waves from the pulse generator. The pulses each represent a force of 170.7 μN over a 1.0 sec pulsewidth and are separated by 2.0 sec. As seen in Fig. 12a, there is good agreement between the measured impulses delivered by the pulse generator to the EFCS and the derived impulses from the NIBS deflection data. Figure 12b shows the delivered impulse as a function of time. As Fig. 12 shows, the data analysis method developed in this study is adequate to resolve discrete forces applied to the impulse balance.

Although attention has been paid to only square-wave impulses to this point, arbitrary impulse shapes can also be investigated. Figure 13a shows a time varying force applied to the thrust stand which might resemble that produced by a PPT or laser ablation mechanism. The derived force obtained from the NIBS position versus time data reproduced the actual applied force reasonably well. Many of the differences in the time varying force have been linked to limitations in the time resolution of the LVDT conditioning unit. Although a factor of perhaps 10 improvement in the LVDT can be reasonably expected, other methods of time resolving the NIBS deflection are being investigated. As shown in Fig. 13b, the applied and derived impulses are nearly identical and compare to within 1.9%.

D. Model Comparison

Figure 14 shows the comparison of the developed model with experimental data for a relatively complicated case of four square-wave impulses applied over a 25 second time period. In Fig. 14a, the model is able to capture the motion of the NIBS for a series of impulses delivered to the balance. The model used the measured and calculated characteristics of the NIBS given in Table 1 as input parameters. Figures 14b and c show the calculated values of the NIBS velocity and acceleration as a function of time. Again, the model compares well with the experimentally derived data obtained from differentiating the NIBS time varying position data. Figure 14d shows the actual time varying forces applied to the NIBS compared to the experimentally derived data. The first pulse was 98.39 μN with a 0.2 sec pulsewidth with the second pulse of the same magnitude separated by 0.3 sec. The second and third pulses were separated by 8.606 sec. The third and fourth pulses were also 98.39 μN with a 0.4 sec pulsewidth separated by 7.055 sec. The integrals under the time varying force curves are shown in Fig. 14e. Again, the

experimental data was able to time resolve the impulse delivery to the NIBS, and the total impulse derived from the NIBS data is within 2.2% of the actual applied impulse.

VII. DISCUSSION

The extension of operating conditions of impulse balances to arbitrary impulse pulsewidth, shape, and magnitude (down to 7 nNs) has been demonstrated with the NIBS using a combination of an analytical code and a data analysis method. Previous studies[2,3] have been limited to data analysis based on the assumption that $\tau \ll T$. For basic research involving new propulsion systems and photon-surface interactions, the characteristic time-dependence of the impulse of a particular process may not be known a priori, making a generalized scheme necessary to time-resolve the impulse delivery to the balance. Also, a torsional impulse balance can deflect the same amount for different total impulses (e.g. see Fig. 9), particularly where the assumption of $\tau \ll T$ is no longer valid. Under similar pulsewidth conditions, an impulse balance can also deflect differently for equivalent total impulses. Therefore, a generalized τ-independent data analysis tool is required.

The NIBS has already demonstrated that it can be used to time-resolve impulses. The real issues now become that of performance. The common measure of an impulse balance's performance is typically that of impulse magnitude resolution. The NIBS has repeatably measured impulses as low as 7nNs and as high hundreds of micro-Newton-seconds, and has consistently derived results that fall within 4.5% (worst case) of the applied impulse. However, when time resolving the forces, it becomes apparent that there are more performance related issues than just the

magnitude of the impulse. Qualitatively, the accuracy of the shape of the time-varying force is of interest. In other words, how closely the derived force matches the applied force over time is important in determining the overall effectiveness of both the TRIM technique and the NIBS itself. Noise and time response of the whole system then become significant issues.

Noise in the measured signal from the NIBS is one of the largest sources of error in the TRIM process. Excessive noise affects the derivatives of the deflection trace and results in noisy time-resolved forces or impulses. There are several sources of noise including external physical vibrations, temperature variations, and electronic noise directly from the LVDT and its signal conditioner. The simplest way to eliminate a significant portion of the electronic noise is the use of a well-tuned LPF. However, LPFs introduce significant time response problems, as they attenuate high frequency components that may actually be part of the signal. Only when time-resolving the forces is not necessary, the LPF provides the best method to obtaining clean signals for basic maximum deflection measurements. In all other cases, the LPF should not be utilized, and the signal processing discussed in Section IV becomes the critical noise reduction method.

In terms of system time response, each component of the NIBS system must be examined. First, the DAQs components play an important role. Often there is a trade-off between resolution and speed. The NIBS system is equipped with both a 16-bit resolution system that samples up to 333KSamples/sec and a 24-bit resolution system that samples up to 60 Samples/sec. Ideally, a high-speed, 24-bit resolution system would be optimal, but has yet to be identified.

Next, the impulse balance itself must be considered for time response issues. The NIBS has been extensively tested with impulses of pulsewidth τ as low as 10^{-7} sec up to minutes in length. Due to time response limitations from the LVDT, the TRIM process only currently provides accurate results for pulsewidths as low as 0.05 seconds. Below this point, aliasing effects make it difficult to discern whether the time-resolution problems are due to the impulse balance or just signal processing artifacts, though the latter is suspected to be the most likely. However, from extensive maximum deflection results, the NIBS behaves as expected across this entire range of pulsewidths. This suggests that the stand is behaving well and does not have time response problems, at least on the order of 10^{-7} seconds.

The last system component to examine for time response issues is the LVDT and its signal conditioner. The time response of an LVDT is typically considered to be at best one tenth of the excitation frequency of the LVDT. For the NIBS, the LVDT is driven at an excitation frequency of 2.5KHz. However, the signal conditioning provided within the controller unit limits the response characteristics further.[13] This accounts for the current time-resolution limitations of the TRIM process. Improvement of the technique described here would be easily achieved through improvements of the overall system time response. While providing excellent displacement resolution, the LVDT signal conditioner was found to have the slowest time response of the entire system, making its replacement desirable. Optical interferometry may offer improved time response over the LVDT system and has been previously investigated, although not for these particular impulse derivation methods. Alternatively, capacitive and other electromagnetic sensors could also be considered.

For actual operation of the NIBS, the error in the TRIM process can be reduced significantly by using a consistent calibration scheme. Since any modification to the impulse balance can change its fundamental characteristics (i.e. I, C, and K), it is necessary to calibrate in the actual test configuration. Using a robust set of calibration tests that maintains a set sampling frequency and covers a wide range of impulses, forces and pulsewidth variations, a correction factor could be determined that would minimize the error. Ideally, calibration sets will be taken before and after any experimental measurements to ensure that the impulse balance remains consistent.

Ultimately, the performance of the impulse balance comes down to repeatability. For the maximum deflection analysis, the experimental error was taken as the standard deviation of between five and ten data points and was typically less than ±2% (i.e. smaller than the symbol size in Figs. 8 and 9 unless otherwise indicated). For the time-resolved impulse analysis, all derivations of total impulse from the deflection measurements have resulted in errors less than ±4.5%, which encapsulates all sources of error including from the applied force. The repeatability of the NIBS data suggests that it is a viable diagnostic tool for the investigation of arbitrarily produced impulses from a variety of devices.

NOMENCLATURE

α	damping term in equations of motion (sec^{-1})
β	frequency term in equations of motion (sec^{-1})
δ	damping ratio, $\ln[x_{max1}/x_{max2}]$
$\mathcal{I}$	impulse, $\int F(t)dt$ (N·sec)

τ	pulsewidth (sec)
θ	angular displacement or deflection (rad)
$\dot{\theta}$	angular velocity (rad/sec)
$\ddot{\theta}$	angular acceleration (rad/sec^2)
ω_{eff}	effective (angular) frequency (sec^{-1})
ω_n	natural (angular) frequency (sec^{-1})
C	viscous damping coefficient (kg·m^2/sec)
F	force (N)
I	moment of inertia (kg·m^2)
K	spring constant (N/m)
M	moment or torque, F · r (N·m)
r	moment arm (m)
T	period (sec)
t	time (sec)
x	linear displacement or deflection (m)
$\dot{x}$ or v	linear velocity (m/sec)
$\ddot{x}$ or a	linear acceleration (m/sec^2)

ACKNOWLEDGEMENTS

This work was supported by the Air Force Research Laboratory, Propulsion Directorate, Space and Missile Propulsion Division (AFRL/PRSA), Edwards AFB, California. One of the authors

(BD) was also supported in part by a graduate assistantship from the Department of Aerospace and Mechanical Engineering at the University of Southern California.

REFERENCES

[1] E. Cubbin, J. Ziemer, E. Choueiri, R. Jahn, Rev. Sci. Instrum. **68**, 2339 (1997).

[2] M. Gamero-Castano, Rev. Sci. Instrum. **74**, 4509 (2003).

[3] T. Haag, Rev. Sci. Instrum. **68**, 2060 (1997).

[4] R.G. Jahn, *Physics of Electric Propulsion* (McGraw-Hill, New York, 1968).

[5] G. Spanjers, K. McFall, F. Gulczinski, and R. Spores, AIAA Paper No. 1996-2723, 32nd Joint Propulsion Conference, July 1996.

[6] R.F. Haglund, *Laser Ablation and Desorption, Experimental Methods in the Physical Sciences*, edited by J. Miller and R. Haglund (Academic Press, San Diego, 1998), Vol. 30, pp. 15-138.

[7] J. Millard, M. Yang, and J. Reilly, J. Phys. Chem. **95**, 4045 (1991)

[8] A. Jamison, A. Ketsdever, and E.P. Muntz, Rev. Sci. Instrum. **73**, 3629 (2002).

[9] N. Selden and A. Ketsdever, Rev. Sci. Instrum. **74**, 5249 (2003).

[10] R.K. Vierck, *Vibration Analysis* (Thomas Y. Crowell, New York, 1979).

[11] C. Gasquet and P. Witomski, *Fourier Analysis and Applications: Filtering, Numerical Computation, Wavelets* (Springer-Verlag, NewYork, 1999).

[12] L.M Jameson, Wavelets Theory and Applications, edited by G. Erlebacher, M.Y. Hussaini, and L.M.Jameson (Oxford University Press, New York, 1996), pp. 1-37.

[13] E.O. Doebelin, Measurement Systems: Application and Design (McGraw-Hill, New York, 1966)

TABLE & FIGURE CAPTIONS

Table 1. General NIBS Characteristics

Figure 1 Schematic of two very different force profiles that result in equivalent total impulses $\mathcal{I}_1=\mathcal{I}_2$. (a) Large initial force with smaller residuals. (b) Constant force of pulsewidth τ.

Figure 2 Schematic of the nano-Newton impulse balance system.

Figure 3 Time-varying deflection trace for a 242 nNs impulse comparing experimental data and the analytical model.

Figure 4 Denoising of LVDT experimental data using wavelet transform and Fourier transform techniques.

Figure 5 Schematic representation of the TRIM process for deriving the time-varying impulse or force from the balance's deflection and its derivatives.

Figure 6 Schematic of NIBS experimental setup and TRIM process for obtaining the derived and applied forces imparted to the impulse balance as a function of time.

Figure 7 TRIM derived impulse versus applied impulse for three dissimilar sets of calibration data.

Figure 8 Comparison of maximum deflection versus applied impulse of the analytical model and experimental deflection data. Error bars represent the standard deviation of at least 10 repeated tests, and are typically smaller than the symbol used.

Figure 9 NIBS maximum deflection as a function of normalized impulse pulsewidth compared to the analytical model results. For $\tau \ll T$, the maximum deflection is constant . The data points represent experimental measurements with error bars showing the standard deviation of at least 10 repeated tests.

Figure 10 Two test cases of equivalent total impulse, with different applied force and pulsewidth. (a) shows that equivalent total impulses can result in different maximum displacements. (b) shows the shape of the applied force for each impulse. (c) shows that the two total impulses are in fact equivalent.

Figure 11 Two test cases of different total impulses that result in the same maximum deflection of the balance as shown in (a). (b) shows the shape of the applied force for each impulse. (c) shows that the two total impulses are in fact different by about a factor of two.

Figure 12 The TRIM process can be used to resolve discrete forces applied to the NIBS. (a) shows the deflection trace corresponding to (b) the time-varying force traces for 2 discrete impulses of 170mN for 1 sec each. (c) shows the resulting total impulse as a function of time.

Figure 13 Plots of (a) the applied and derived forces as a function of time for an arbitrary impulse, and (b) the corresponding applied and derived total impulses.

Figure 14 Comparison of the analytical model with the experimental measurements for multiple pulses of varying pulsewidth. The plots show the sequence of steps in the TRIM process. (a) The balance's deflection, (b) velocity, and (c) acceleration. (d) The time varying force, and (e) the total impulse as a function of time.

Table 1

Parameter	Value	Error (+/-)
Moment of Inertia, **I**	0.03184 kg m^2	0.00010 kg m^2
Damping Coefficient, **C**	0.00023 kg m^2/s	0.00002 kg m^2/s
Spring Constant, **K**	0.20034 N/m	0.00150 N/m
Period, **T**	2.49 s	0.01 s
Angular Frequency, ω_{eff}	2.523 s^{-1}	0.010 s^{-1}
Damping Ratio, δ	0.0090	0.0009
Moment Arm, **r**	0.4635 m	0.0005 m

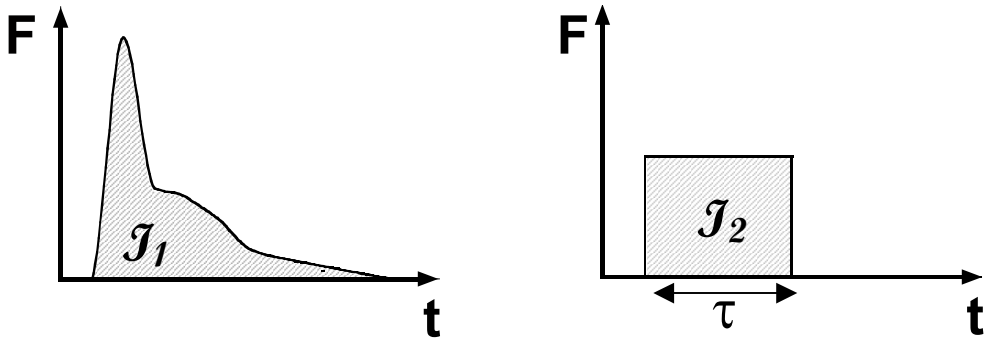

(a) (b)

Figure 1

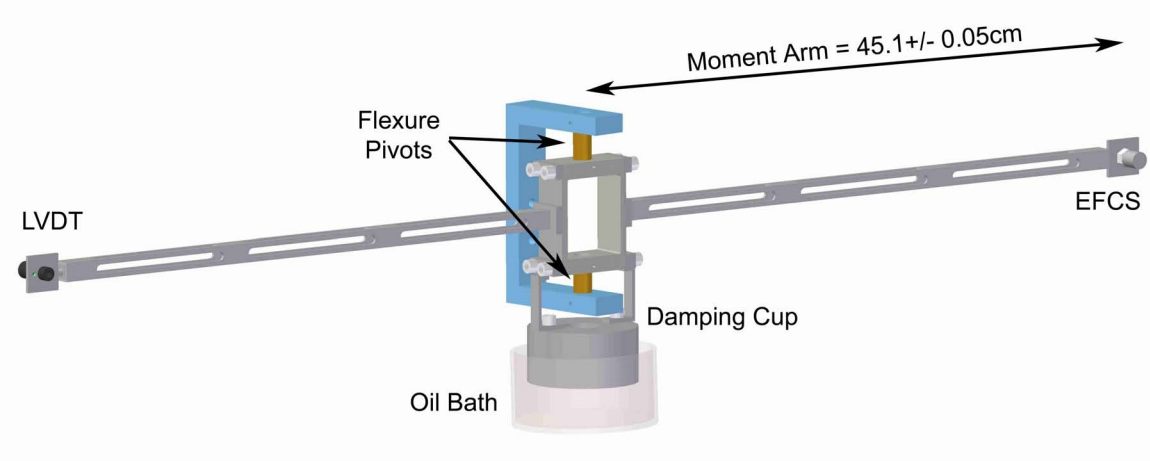
Moment Arm = 45.1+/- 0.05cm
Flexure
Pivots
LVDT
EFCS
Damping Cup
Oil Bath

Figure 2

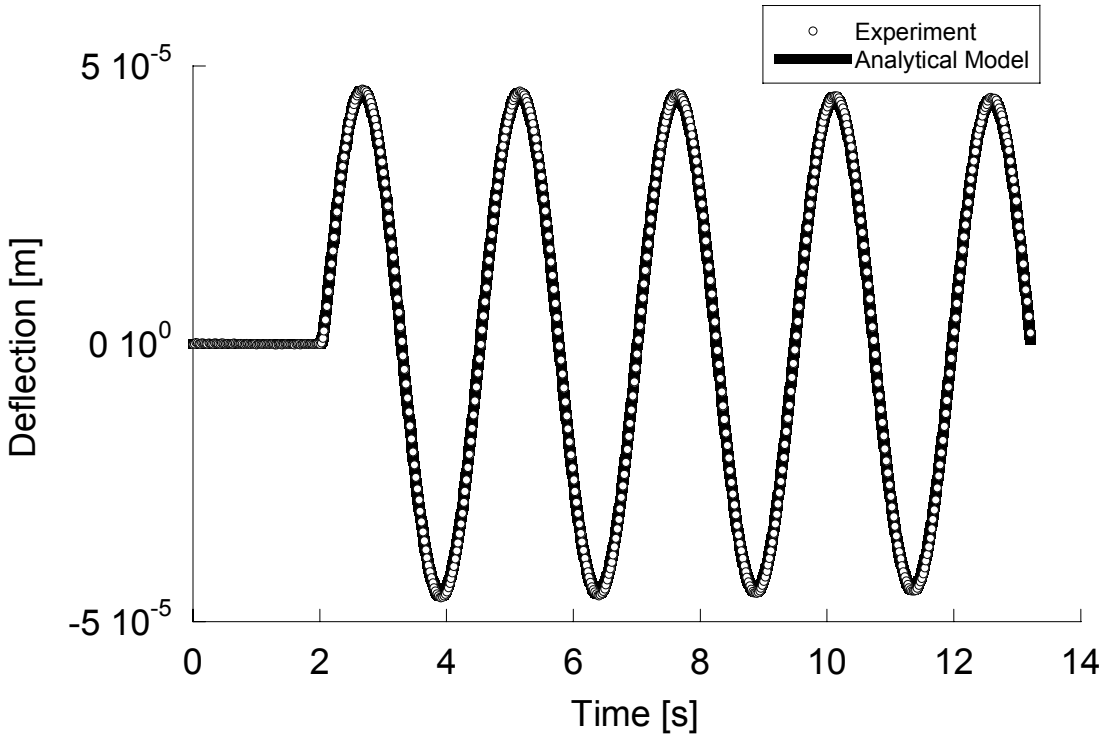
Experiment
Analytical Model
5 10-5
0 100
-5 10-5
Deflection [m]
0
2
4
6
8
10
12
14
Time [s]

Figure 3

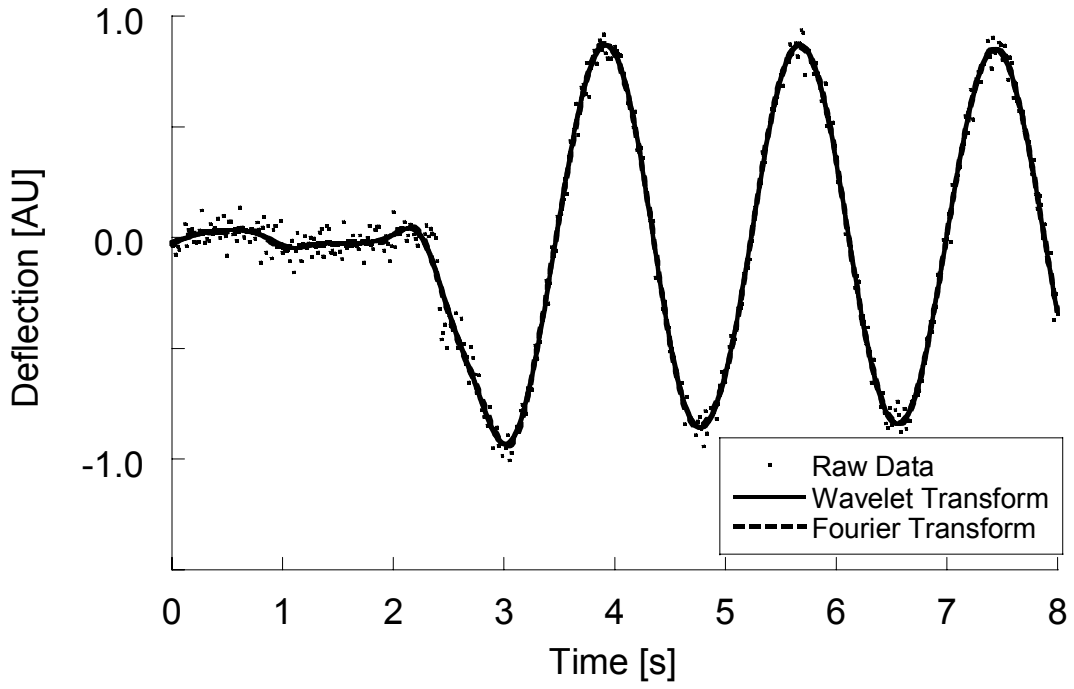
1.0
0.0
-1.0
Deflection [AU]
0
1
2
3
4
5
6
7
8
Time [s]
Raw Data
Wavelet Transform
Fourier Transform

Figure 4

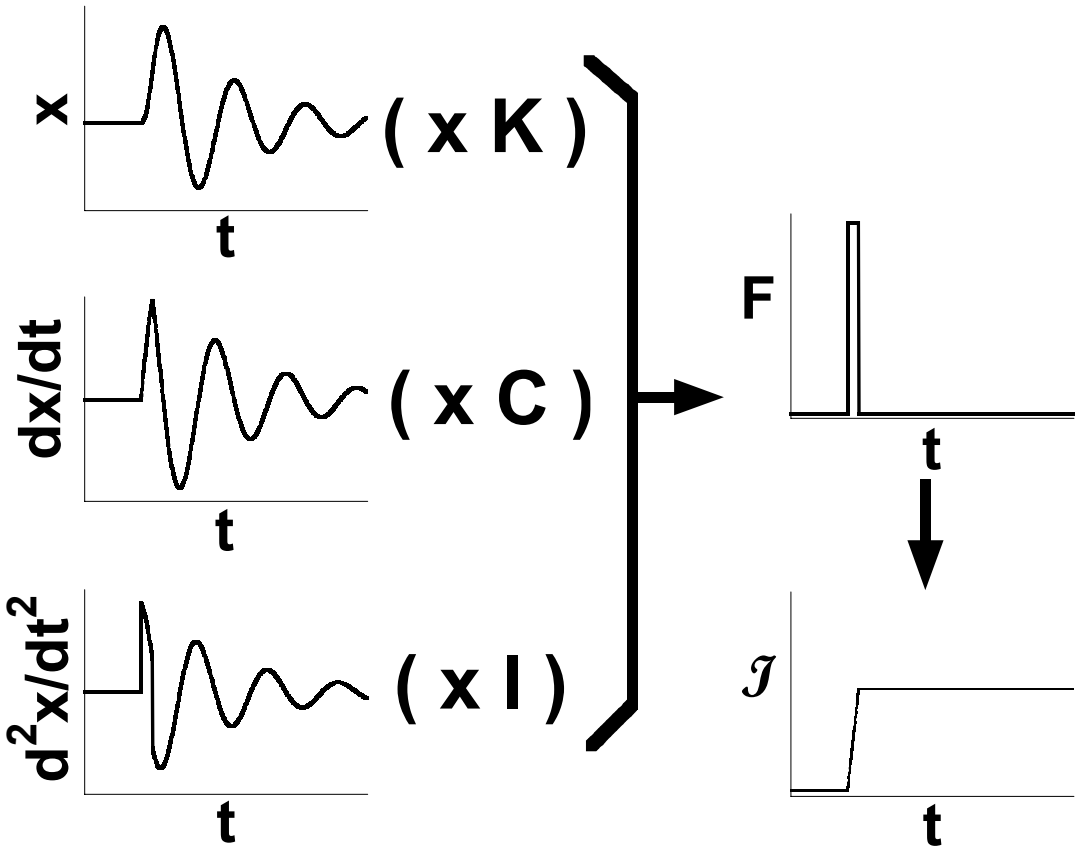

Figure 5

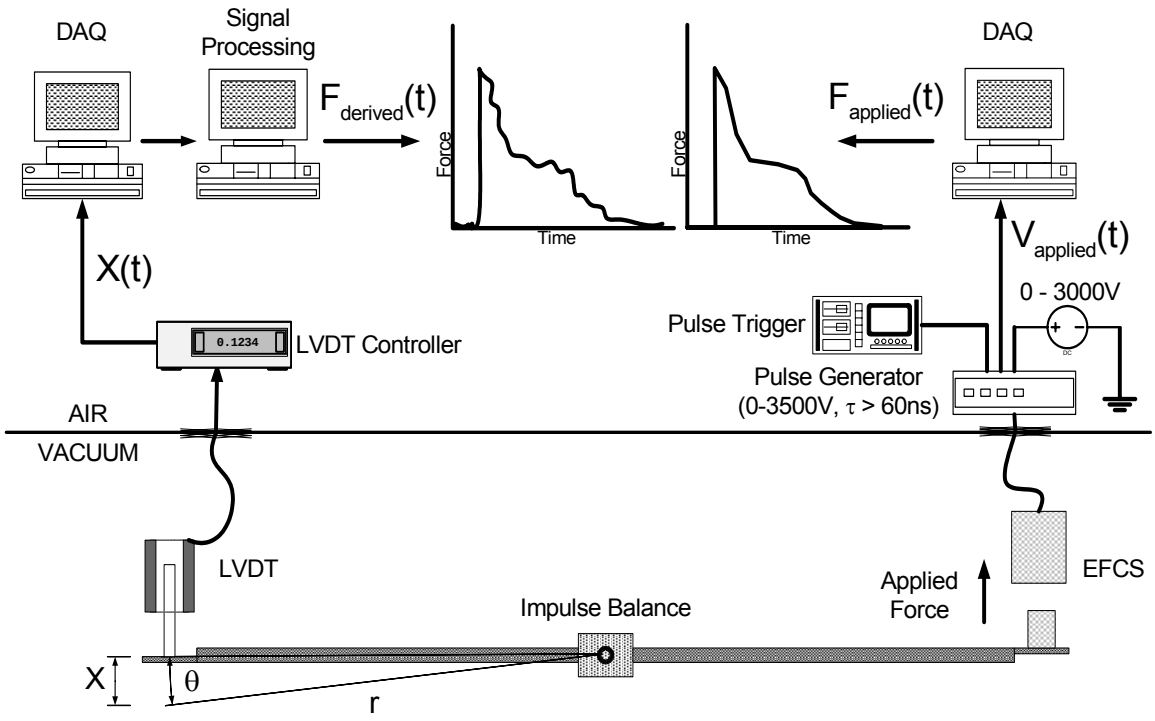
DAQ
Signal Processing
$F_{derived}(t)$
Force
Time
Force
Time
$F_{applied}(t)$
DAQ
$V_{applied}(t)$
0 - 3000V
X(t)
0.1234
LVDT Controller
Pulse Trigger
Pulse Generator
(0-3500V, τ > 60ns)
AIR
VACUUM
LVDT
Impulse Balance
Applied Force
EFCS
X
θ
r

Figure 6

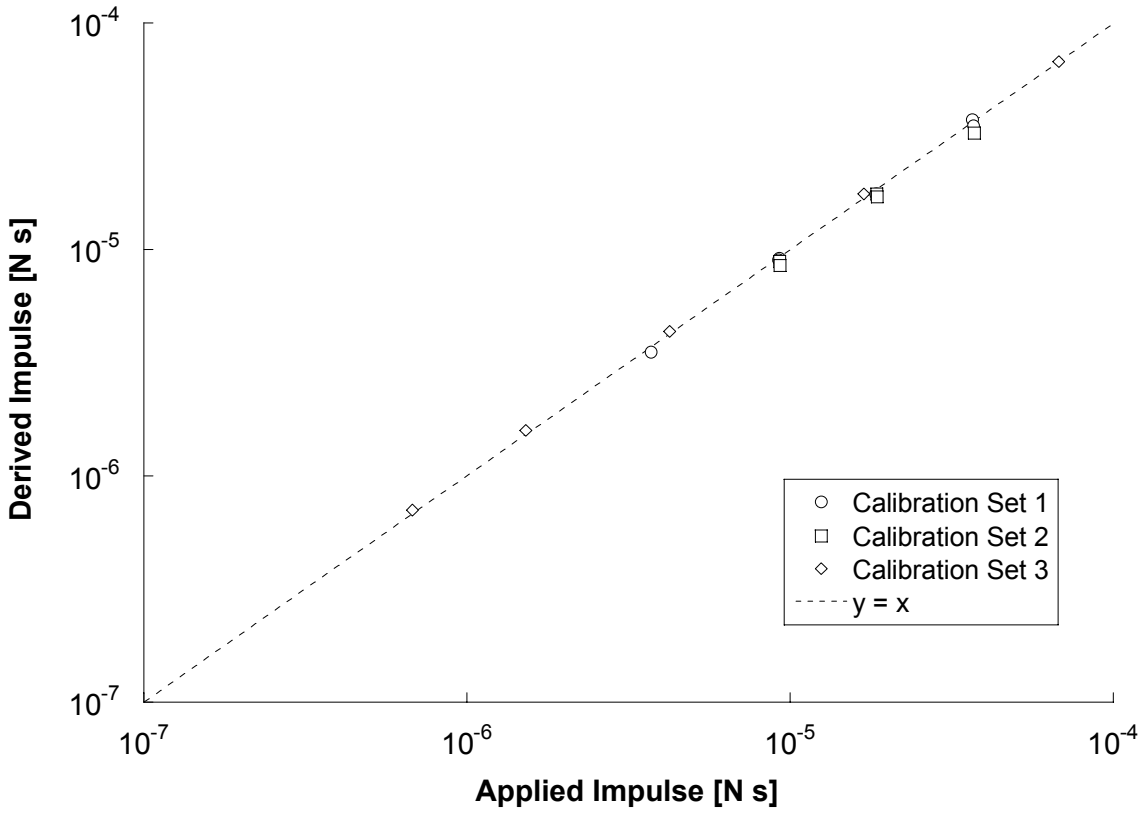
Derived Impulse [N s]
Applied Impulse [N s]
10^-4
10^-5
10^-6
10^-7
Calibration Set 1
Calibration Set 2
Calibration Set 3
y = x

Figure 7

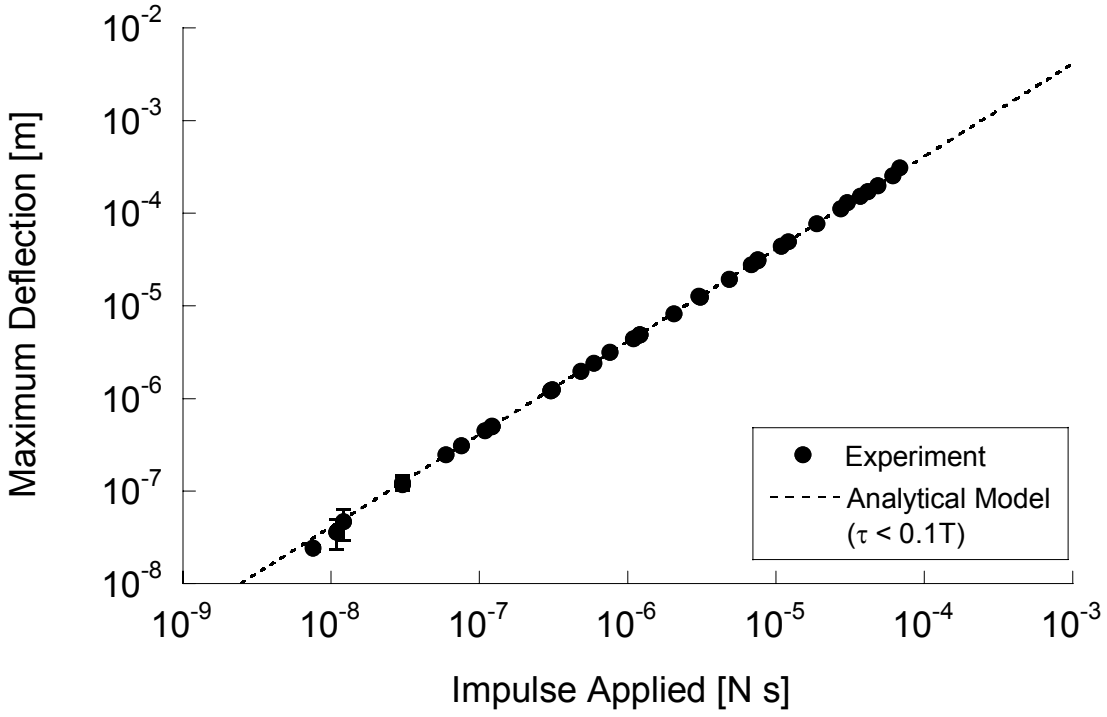
Maximum Deflection [m]
10-2
10-3
10-4
10-5
10-6
10-7
10-8
10-9
10-8
10-7
10-6
10-5
10-4
10-3
Impulse Applied [N s]
Experiment
Analytical Model
(τ < 0.1T)

Figure 8

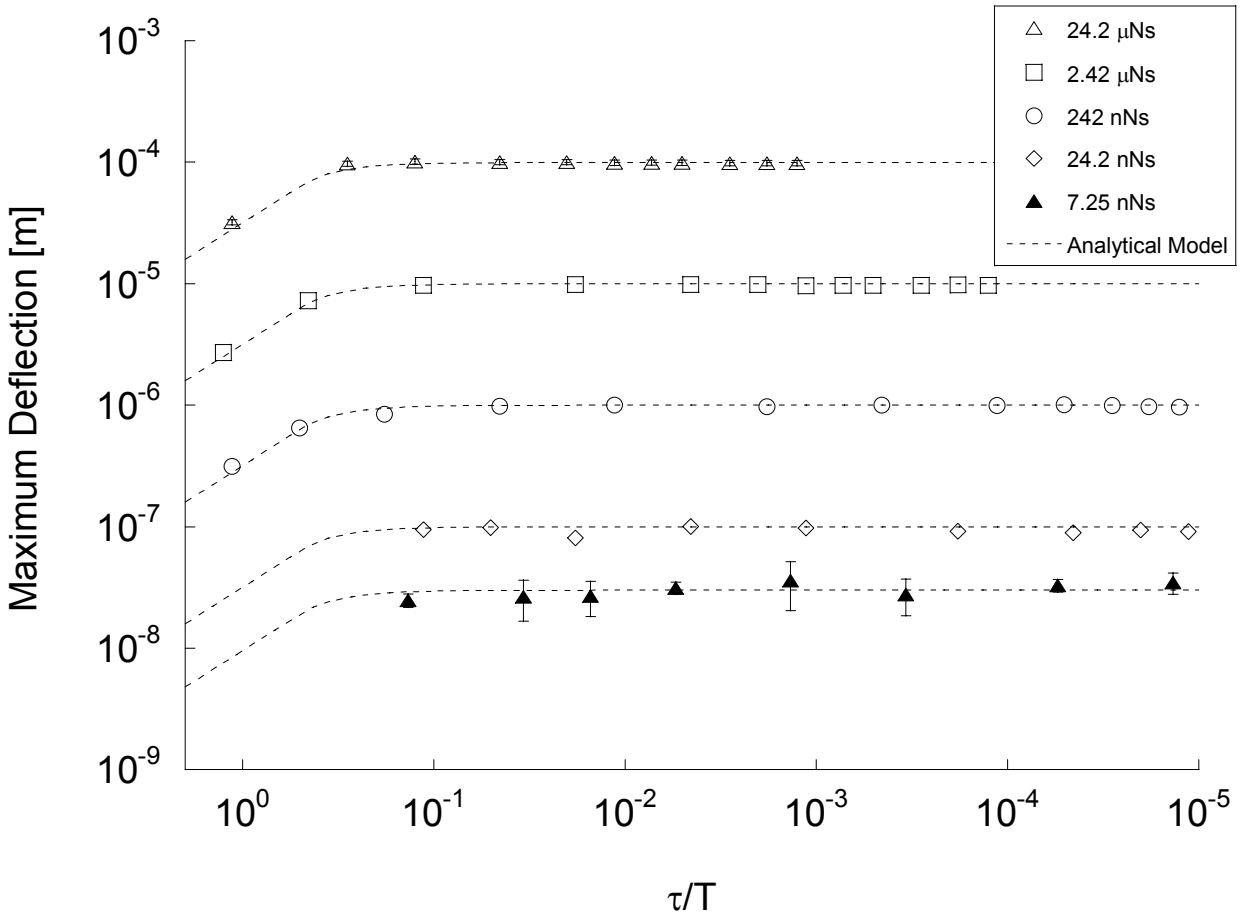
Maximum Deflection [m]
10-3
10-4
10-5
10-6
10-7
10-8
10-9
100
10-1
10-2
10-3
10-4
10-5
τ/T
24.2 μNs
2.42 μNs
242 nNs
24.2 nNs
7.25 nNs
Analytical Model

Figure 9

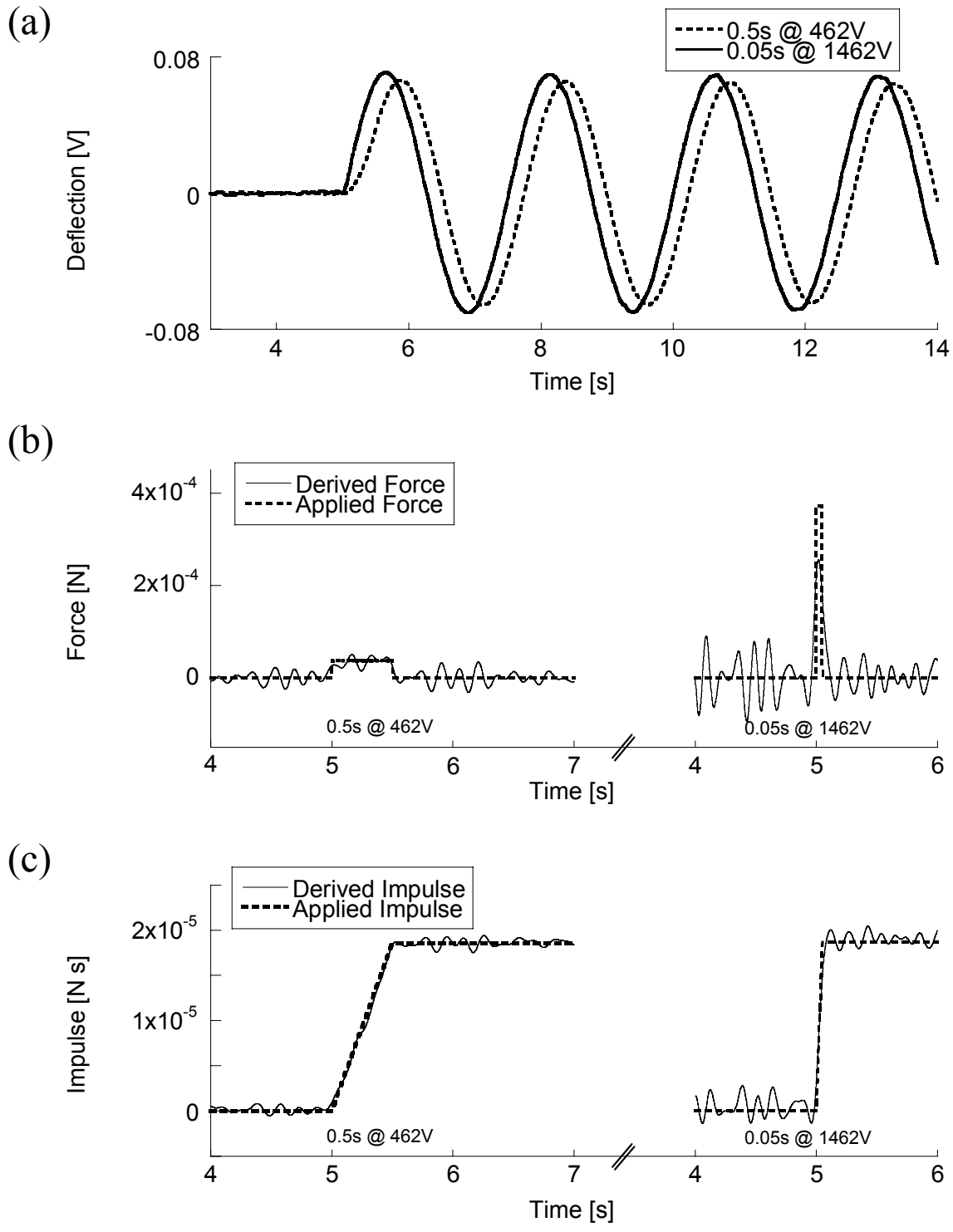
(a)
0.5s @ 462V
0.05s @ 1462V
0.08
0
-0.08
Deflection [V]
4
6
8
10
12
14
Time [s]
(b)
Derived Force
Applied Force
4x10-4
2x10-4
0
Force [N]
0.5s @ 462V
0.05s @ 1462V
4
5
6
7
4
5
6
Time [s]
(c)
Derived Impulse
Applied Impulse
2x10-5
1x10-5
0
Impulse [N s]
0.5s @ 462V
0.05s @ 1462V
4
5
6
7
4
5
6
Time [s]

Figure 10

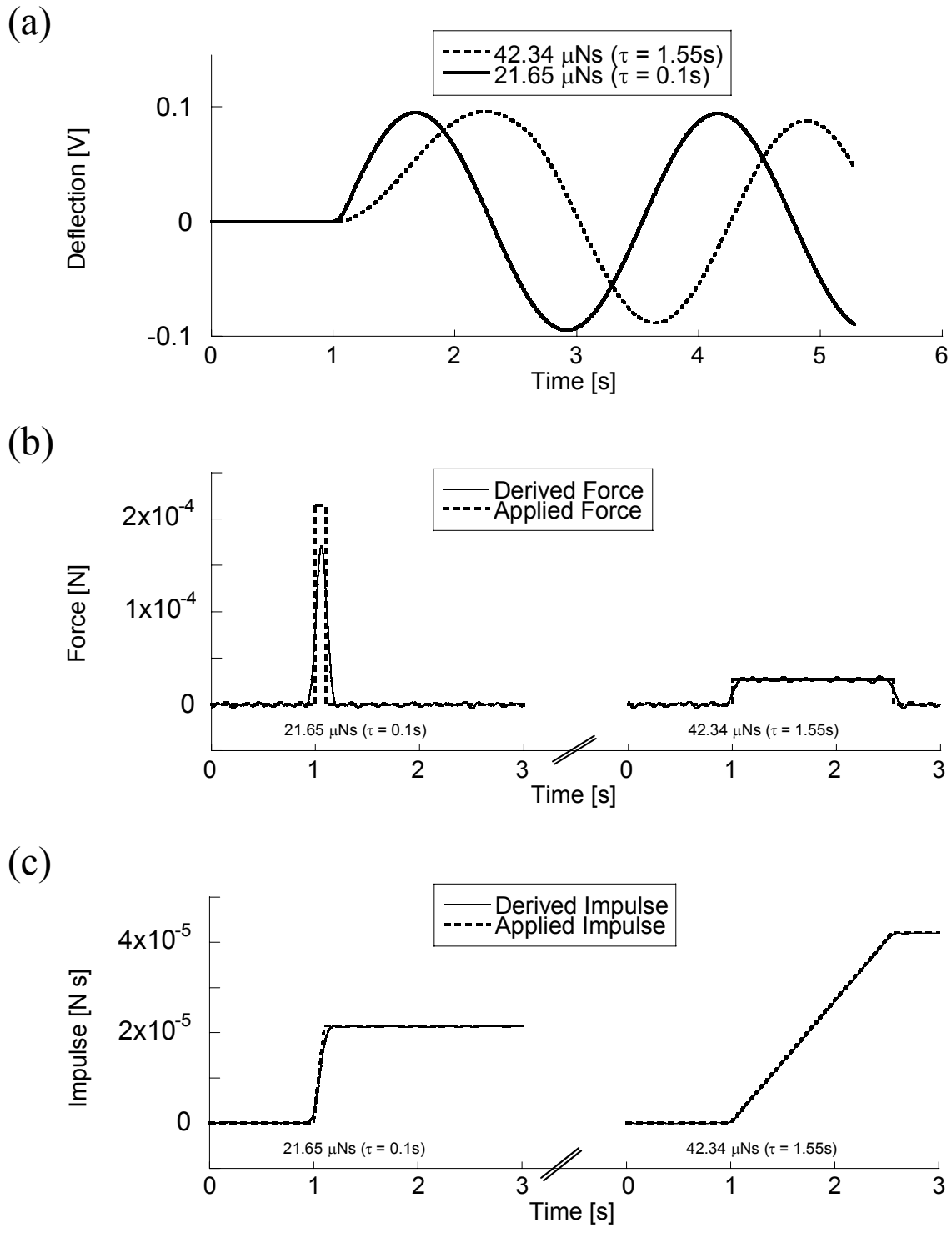
(a)
42.34 μNs (τ = 1.55s)
21.65 μNs (τ = 0.1s)
Deflection [V]
0.1
0
-0.1
0
1
2
3
4
5
6
Time [s]
(b)
Derived Force
Applied Force
Force [N]
2x10-4
1x10-4
0
21.65 μNs (τ = 0.1s)
42.34 μNs (τ = 1.55s)
0
1
2
3
0
1
2
3
Time [s]
(c)
Derived Impulse
Applied Impulse
Impulse [N s]
4x10-5
2x10-5
0
21.65 μNs (τ = 0.1s)
42.34 μNs (τ = 1.55s)
0
1
2
3
0
1
2
3
Time [s]

Figure 11

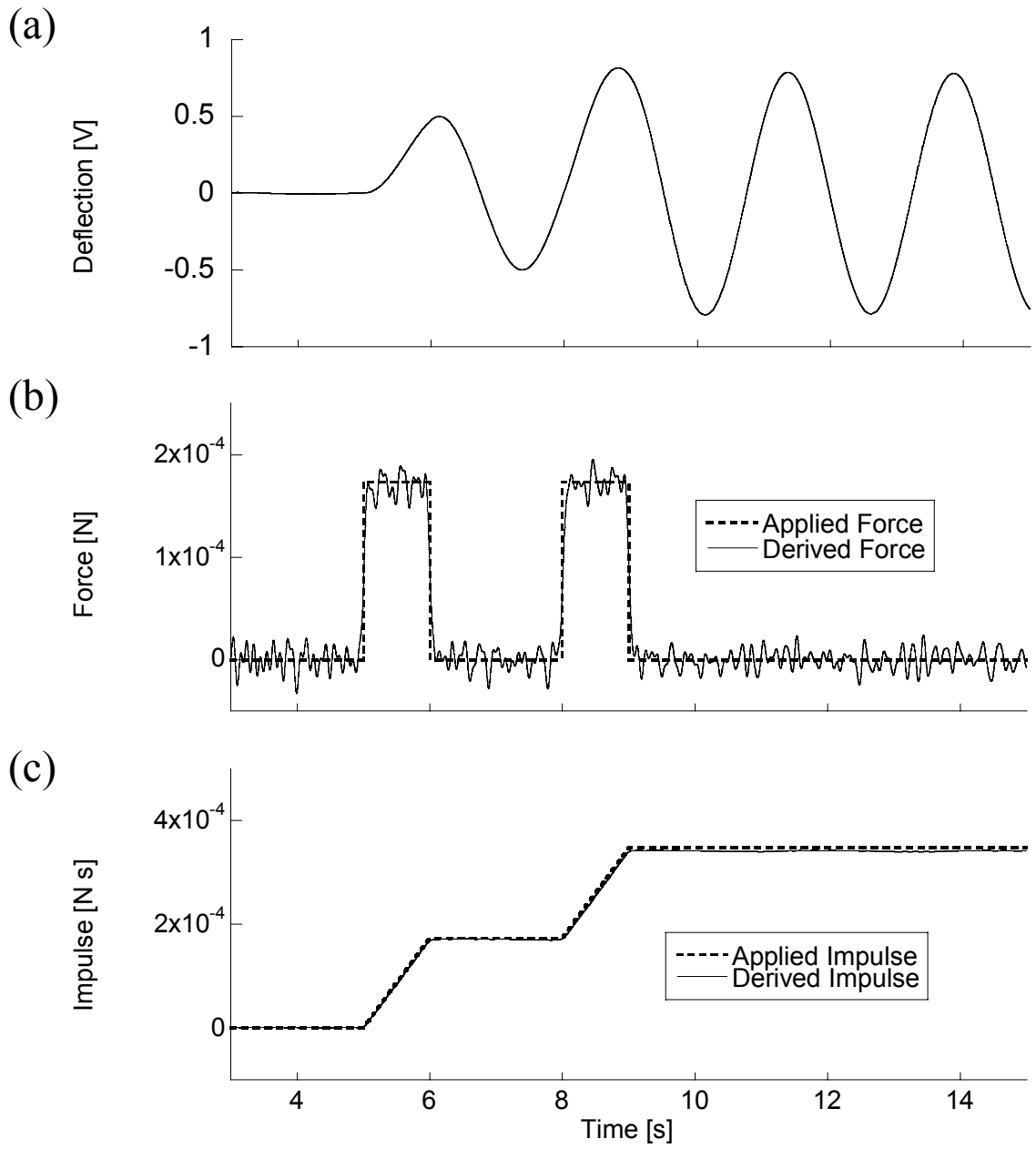
(a)
Deflection [V]
1
0.5
0
-0.5
-1
(b)
Force [N]
2x10-4
1x10-4
0
Applied Force
Derived Force
(c)
Impulse [N s]
4x10-4
2x10-4
0
Applied Impulse
Derived Impulse
4
6
8
10
12
14
Time [s]

Figure 12

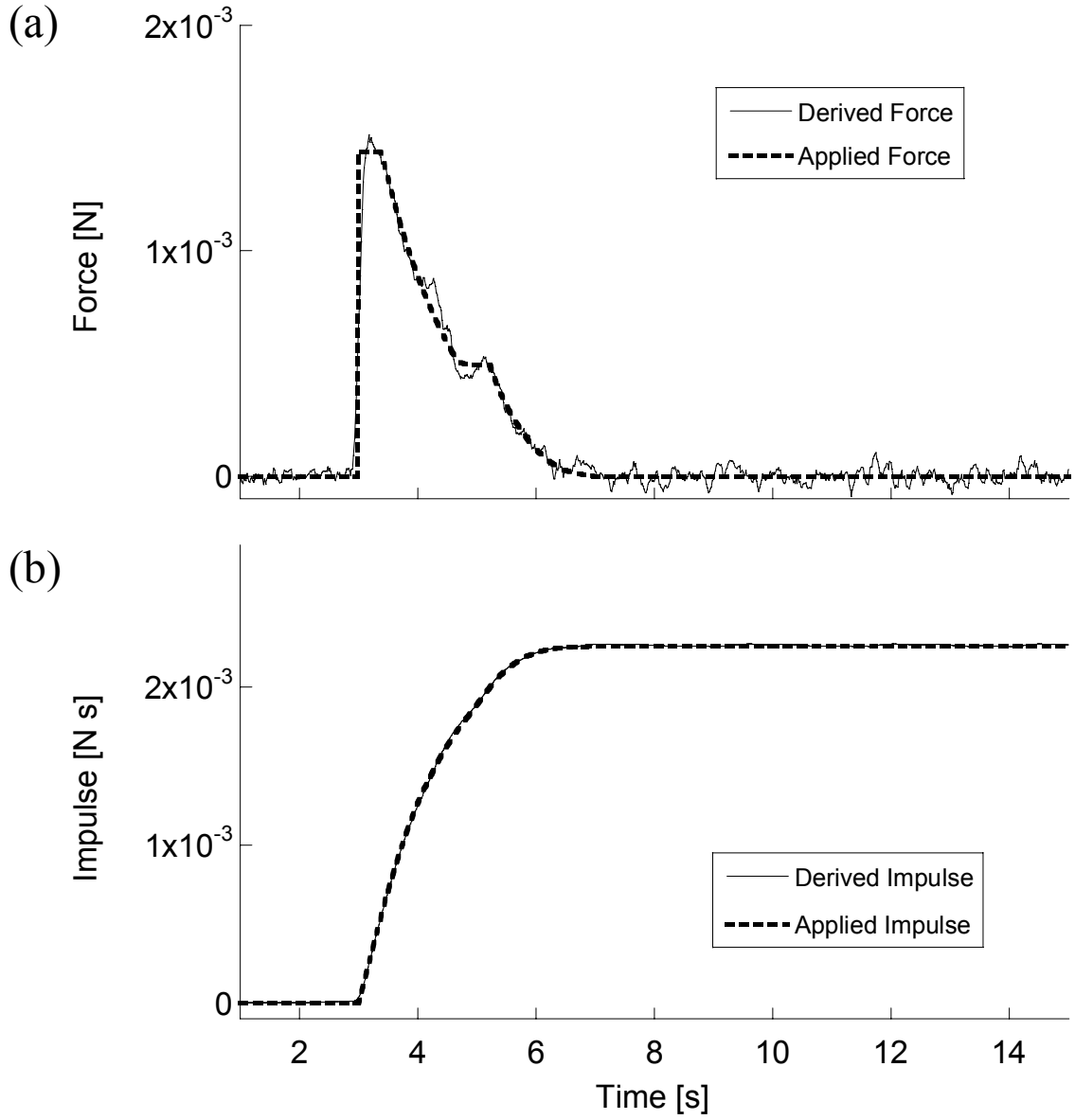
(a)
2x10-3
1x10-3
0
Force [N]
Derived Force
Applied Force
(b)
2x10-3
1x10-3
0
Impulse [N s]
Derived Impulse
Applied Impulse
2
4
6
8
10
12
14
Time [s]

Figure 13

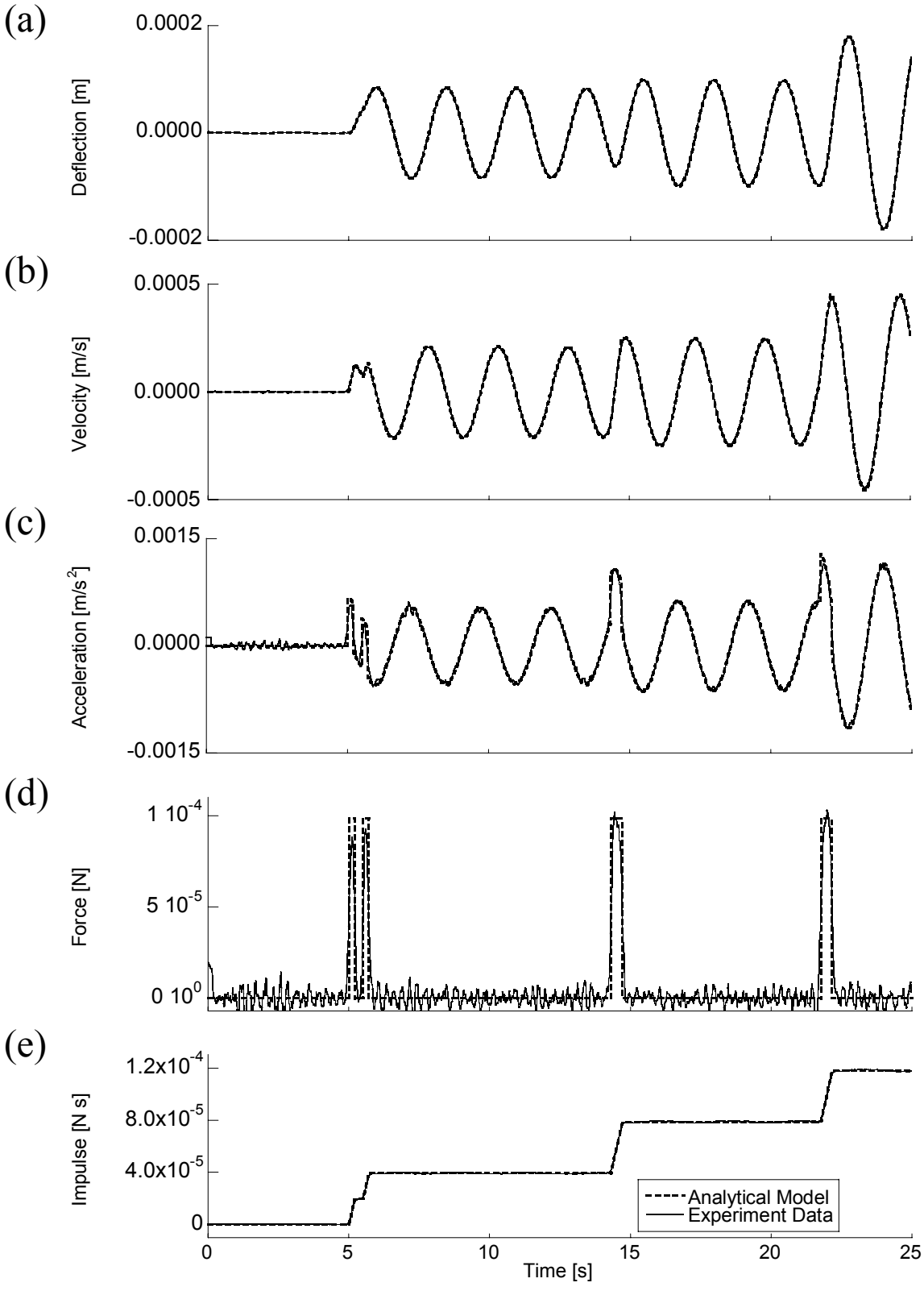
(a)
0.0002
0.0000
-0.0002
Deflection [m]
(b)
0.0005
0.0000
-0.0005
Velocity [m/s]
(c)
0.0015
0.0000
-0.0015
Acceleration [m/s^2]
(d)
1 10^{-4}
5 10^{-5}
0 10^0
Force [N]
(e)
1.2x10^{-4}
8.0x10^{-5}
4.0x10^{-5}
0
Impulse [N s]
Analytical Model
Experiment Data
0
5
10
15
20
25
Time [s]

Figure 14